Linear stability analysis for the onset of convection during microwave heating of oil confined within horizontal plates

Madhuchhanda Bhattacharya and Tanmay Basak

Citation: Journal of Applied Physics **105**, 024906 (2009); doi: 10.1063/1.3066236
View online: http://dx.doi.org/10.1063/1.3066236
View Table of Contents: http://scitation.aip.org/content/aip/journal/jap/105/2?ver=pdfcov
Published by the AIP Publishing

Linear stability analysis for the onset of convection during microwave heating of oil confined within horizontal plates

Madhuchhanda Bhattacharya[1] and Tanmay Basak[2,a)]
[1]*D29-81 Adyar Avenue, Indian Institute of Technology Madras, Chennai 600 036, India*
[2]*Department of Chemical Engineering, Indian Institute of Technology Madras, Chennai 600036, India*

(Received 28 April 2008; accepted 3 December 2008; published online 27 January 2009)

This work performs linear stability analysis to investigate the onset of convection due to microwave incidences in a horizontal oil layer. The probability of onset has been characterized in terms of critical Rayleigh number (Ra_c), while the microwave power required to initiate convection has been quantified in terms of modified Rayleigh number ($\overline{Ra}_c$). The associated convection cell size has been illustrated by critical wave number (k_c). These critical numbers (Ra_c, $\overline{Ra}_c$, and k_c) have been determined for the entire spectrum of oil thicknesses ranging from thin to thick samples and various possible microwave source configurations starting from one sided to distributed incidences. It has been shown that the critical numbers oscillate with oil thickness in intermediate regime indicating preferential onset for specific oil thicknesses. It has also been shown that microwave source configuration plays an important role in controlling the onset of convection. Finally, the variations of Ra_c and k_c have been correlated to the spatial patterns of absorbed microwave power within oil, while modified Rayleigh numbers are shown to follow the qualitative trends of ΔT_s, where ΔT_s is the base state temperature difference between top and bottom plate. The results are useful not only for forecasting the onset but also for controlling onset of convection by selecting suitable experimental parameters. © *2009 American Institute of Physics*. [DOI: 10.1063/1.3066236]

I. INTRODUCTION

Microwave heating of oil has received significant attention in various industrial processes ranging from food processing to oil recovery[1–10] due to the possibility of faster processing. Microwaves cause volumetric heating within oil, where the spatial patterns of internal heat sources depend on various design parameters such as dielectric properties, thickness, microwave source configurations, etc.[11–22] Based on these parameters, microwave induced internal heat sources may either be uniformly distributed or exhibit spatial oscillations or attenuate exponentially from the edges and may preferentially trigger natural convection. The onset of natural convection is important in the context of resulting temperature profiles[23,24] within oil, which may be one of the key issues in implementing microwave heating in various processes. Since spatial distributions of internal heat sources vary widely with design parameters, it is important to characterize the onset of convection in terms of critical Rayleigh (Ra_c) and wave (k_c) numbers in order to answer the fundamental question: When natural convection sets in during microwave heating of oil?

The onset of natural convection in horizontally confined fluid layer with internal heat sources has been analyzed by earlier researchers in various other context of motion in the atmosphere of Earth[25] and Venus,[26] solar heating,[27] convection in magnetic fluid,[28] and Joule heating of conducting fluid.[29–32] Various aspects of onset such as effect of boundary conditions,[33–35] effect of temperature dependent viscosity,[36] or the effect of distributed heat sources[37,38] have also been studied by earlier researchers. However, most of the earlier works considered the internal heat sources to be uniformly distributed within the domain except few studies,[36–38] where internal heat sources were assumed to be exponentially decaying from either top or bottom surface. These spatial patterns may represent some of the configurations of microwave heating of oil. For example, thin oil samples with thickness less than the wave length (λ_m) absorb microwave power uniformly. On the other hand, microwave power attenuates exponentially within thick oil samples, where oil thickness is greater than penetration depth (D_p). However, in between thin and thick oil samples, microwave induced internal heat sources exhibit highly nonlinear spatial patterns, which evolve with oil thickness. In this regime, spatial patterns of microwave induced heat sources are strong function of microwave source configurations and exhibit local intensification.[19,20] Also, the region of local intensification of absorbed power oscillates between top and bottom halves of the samples as oil thickness varies in the intermediate regime.[19,20] This is in contrast with the absorbed power characteristics in thin and thick samples, where the region of power intensification is confined either at top or bottom of the sample based on microwave source configurations. One interesting observation reported by earlier researchers is that local intensification of internal heat source either facilitate or delay the onset of convection based on the orientation of heat source.[38] Therefore, the critical Rayleigh and wave numbers are expected to be nonlinear function of oil thickness and microwave source configurations in intermediate regime, where natural convection may set in counterintuitively. Thus, it is important to quantify the effect of various design param-

a)Author to whom correspondence should be addressed. Electronic addresses: madhuchhanda_bhattacharya@yahoo.co.in and tanmay@iitm.ac.in.

eters on the onset of convection in terms of Ra_c and k_c over the entire span of thin to thick oil samples, which are yet to appear in literature.

The analysis of the onset of natural convection in presence of microwave radiations is complex due to the fact that microwave induced heat source profiles vary with various design parameters mentioned above and enforce the requirement of solving momentum and energy balance equations in conjunction with Helmholtz equations for the induced electric field taking into account the transmissions and reflections at the boundaries. One such attempt has been made in the earlier work,[39] where linear stability analysis was performed for microwave hating of ethyl alcohol confined between two horizontal plates by solving coupled momentum, energy and Helmholtz equations. The authors examined the effect of boundary conditions and the rigidity of the surfaces on neutral stability curves. The authors also reported the variations of Ra_c and k_c with sample thicknesses (L) within the range $L/\lambda_m \leqslant 0.8$ (equivalent to $L/D_p \leqslant 0.44$), which is much below the thick sample limit given by $L/D_p \geqslant 3$. Moreover, authors considered only one type of microwave source configuration, i.e., top incidence and overlooked other possible microwave source configurations.

This work analyzes microwave induced onset of natural convection within a horizontal oil layer over the entire spectrum of oil thicknesses and microwave source configurations (one sided or distributed incidences). The critical Rayleigh and wave numbers have been determined by performing linear stability analysis of coupled momentum, energy, and Helmholtz equations. The effect of various configurations of microwave sources on Ra_c and k_c in thin, intermediate, and thick oil samples has been investigated in details. This work also analyzes the physics of nonlinear variations of Ra_c and k_c and relate them to the spatial distributions of microwave induced heat source patterns.

II. GOVERNING EQUATIONS FOR MICROWAVE HEATING

The governing conservation, momentum, and energy balance equations for microwave induced natural convection in oil may be written as

$$\nabla^* \cdot \mathbf{V} = 0, \tag{1a}$$

$$\rho_0 \frac{\partial \mathbf{V}}{\partial t} + \mathbf{V} \cdot \nabla^* \mathbf{V} = -\nabla^* P - \rho_0[1 - \beta(T - T_0)]g\mathbf{e_z} + \mu \nabla^{*2}\mathbf{V}, \tag{1b}$$

$$\rho_0 C_p \left[\frac{\partial T}{\partial t} + \mathbf{V} \cdot \nabla^* T \right] = \gamma \nabla^{*2} T + Q(Z), \tag{1c}$$

where $\mathbf{V}$, P, and T denote state variables as velocity vector, pressure, and temperature, respectively, ∇^{*2} is the Laplacian operator in Cartesian coordinate system, C_p is the specific heat, β is the thermal expansion factor, ρ_0 is the density of oil at $T=T_0$, μ is the viscosity, γ is the thermal conductivity, and $Q(Z)$ is the internal heat source distribution due to microwave power absorption. Here, it is assumed that the buoyancy driven flow within oil can be modeled by Boussinesq approximation with constant thermal and material properties. The oil is confined between two parallel semi-infinite horizontal plates a distance L apart and microwave is incident from top and bottom, as shown in Fig. 1. It may be noted that microwave power absorption within such semi-infinite configurations can be assumed to be one dimensional[14–16,40–44] and $Q(Z)$ becomes the function of only vertical position. The governing equation for microwave propagation within semi-infinite dielectric and the expression for $Q(Z)$ are given in Sec. II A. Here, It is assumed that the plates are perfectly impermeable to flow. It is also assumed that the bottom plate is thermally insulated and top plate is isothermal with $T=T_0$. With origin of Cartesian coordinate $\{X, Y, Z\}$ at the center of the domain consisting of oil confined within two plates (see Fig. 1), the associated boundary conditions in vertical direction can be written as

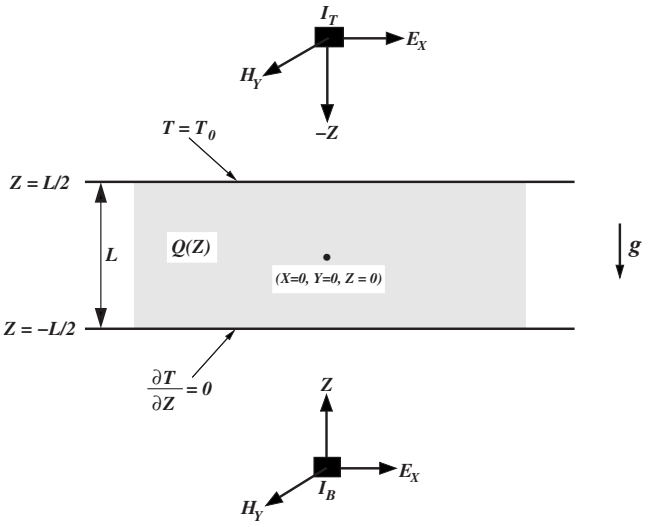

FIG. 1. Computational domain of oil layer confined between two horizontal plates exposed to microwave radiations of I_T and I_B from top and bottom, respectively. The coordinate system and the thermal boundary conditions are shown in the figure.

$$\mathbf{V} = \mathbf{0} \quad \text{at } Z = \pm L/2 \quad \text{and} \quad \begin{cases} \dfrac{\partial T}{\partial Z} = 0 & \text{at } Z = -L/2 \\ T = T_0 & \text{at } Z = L/2. \end{cases} \tag{2}$$

It may be noted that Eqs. (1) and (2) can exhibit a steady quiescent solution ($\mathbf{V}=0$) for small enough heat source. Let us denote this conduction state as $[P_s(Z), T_s(Z)]$ such that

$$\frac{dP_s}{dZ} = -\rho_0[1 - \beta(T_s - T_0)]g, \tag{3a}$$

$$\gamma \frac{d^2 T_s}{dZ^2} = -Q(Z), \tag{3b}$$

with the associated boundary conditions as

$$\frac{\partial T_s}{\partial Z} = 0 \quad \text{at } Z = -L/2, \quad T_s = T_0 \quad \text{at } Z = L/2. \tag{4}$$

Then, the convective flow induced by any larger heat source can be represented as perturbation to this base state as

$$\mathbf{V} = \mathbf{V}'(X,Y,Z,t), \quad P = P_s(Z) + P'(X,Y,Z,t),$$
$$T = T_s(Z) + T'(X,Y,Z,t). \tag{5}$$

Substituting Eq. (5) in Eq. (1) and using L, L^2/α_0, α_0/L, $\rho_0\alpha_0^2/L^2$, and $\Delta T_s \equiv T_s(Z=-L/2)-T_0$ as the scales for length, time, velocity, pressure, and temperature, respectively, the linearized evolution equations for the dimensionless perturbation functions can be written as

$$\nabla \cdot \mathbf{v}' = 0, \tag{6a}$$

$$\frac{\partial \mathbf{v}'}{\partial \tau} = -\nabla p' + \mathrm{Ra}\,\mathrm{Pr}\,\theta' \mathbf{e_z} + \mathrm{Pr}\nabla^2 \mathbf{v}', \tag{6b}$$

$$\frac{\partial \theta'}{\partial \tau} + w' \frac{d\theta_s}{dz} = \nabla^2 \theta'. \tag{6c}$$

Here, $\alpha_0 = \gamma/\rho_0 C_p$ is the thermal diffusivity at $T=T_0$, $\mathbf{v}'$, p' and θ' are dimensionless perturbation functions for velocity, pressure, and temperature, respectively, with w' in Eq. (6c) denoting the perturbation function for vertical velocity. In addition, $\{x,y,z\}$ is the dimensionless coordinate and τ is the dimensionless time. The dimensionless numbers in Eq. (6) are Prandtl number as $\mathrm{Pr} = \nu_0/\alpha_0$ and Rayleigh number as $\mathrm{Ra} = L^3 g\beta\Delta T_s/\nu_0\alpha_0$, with $\nu_0 = \mu/\rho_0$ as the kinematic viscosity at $T=T_0$. Eliminating pressure from Eqs. (6a) and (6b), the governing equation for the velocity perturbation vector can be written as

$$\frac{\partial(\nabla^2 \mathbf{v}')}{\partial \tau} = \mathrm{Ra}\,\mathrm{Pr}\left(\nabla^2 \theta' \mathbf{e_z} - \nabla \frac{\partial \theta'}{\partial z}\right) + \mathrm{Pr}(\nabla^2)^2 \mathbf{v}'. \tag{7}$$

It may be noted that only perturbation function for vertical velocity is required to determine the perturbation function for temperature.

Expanding the perturbation functions as

$$\{\mathbf{v}', \theta'\} = \{\bar{\mathbf{v}}(z), \bar{\theta}(z)\} e^{i(k_x x + k_y y) + \sigma\tau}, \tag{8}$$

the perturbation equations for temperature and vertical velocity can be transformed into the following:

$$\left(\frac{d^2}{dz^2} - k^2 - \frac{\sigma}{\mathrm{Pr}}\right)\left(\frac{d^2}{dz^2} - k^2\right)\bar{w} = \mathrm{Ra}\, k^2 \bar{\theta}, \tag{9a}$$

$$\left(\frac{d^2}{dz^2} - k^2 - \sigma\right)\bar{\theta} = \frac{d\theta_s}{dz}\bar{w}, \tag{9b}$$

where k is the horizontal wave number given by $k^2 = k_x^2 + k_y^2$. The associated boundary conditions can be written as

$$\bar{w} = \frac{d\bar{w}}{dz} = 0 \quad \text{at } z = \pm 1/2 \quad \text{and} \quad \begin{cases} \dfrac{d\bar{\theta}}{dz} = 0 & \text{at } z = -1/2 \\ \bar{\theta} = 0 & \text{at } z = 1/2. \end{cases} \tag{10}$$

Thus, the critical Rayleigh and wave number can be determined by solving the eigenvalue problem given by Eqs. (9) and (10) supplemented with the expression for $d\theta_s/dz$, which can be obtained from the expression for base state temperature profiles (T_s). The closed form expression for $T_s(z)$ can be determined by integrating Eq. (3b) along with Eq.(4) once the closed form expression for microwave power absorption is known as outlined in the following section.

A. Expressions for microwave induced internal heat source and base state temperature profiles

The propagation of microwave within oil is characterized by wavelength (λ_m) and penetration depth (D_p), which in turn depends on the dielectric constant (κ_m') and dielectric loss (κ_m'') of oil as

$$\lambda_m = \frac{\sqrt{2}}{f\sqrt{\mu_0\epsilon_0}\left[\sqrt{\kappa_m'^2 + \kappa_m''^2} + \kappa_m'\right]^{1/2}}, \tag{11a}$$

$$\text{and} \quad D_p = \frac{\sqrt{2}}{2\pi f\sqrt{\mu_0\epsilon_0}\left[\sqrt{\kappa_m'^2 + \kappa_m''^2} - \kappa_m'\right]^{1/2}}, \tag{11b}$$

where f is the frequency of radiation, μ_0 is the free space permeability, and ϵ_0 is the free space permittivity. In general, κ_m' and κ_m'' are functions of frequency of radiations. However, most of the thermal applications of microwave operate at 2450 MHz at which the dielectric properties of a typical edible oil are reported to be $\kappa_m' \approx 2.8$ and $\kappa_m'' \approx 0.15$.[13,14] Using these values, the wavelength and penetration depth within oil at 2450 MHz frequency are obtained from Eq. (11) as $\lambda_m = 7.31$ cm and $D_p = 43.47$ cm. von Hippel[45] presented dielectric data of various oils as a function of temperature and it is found that dielectric properties do not vary significantly for a temperature range of 30–100 °C. Therefore, the temperature dependency of dielectric properties has been neglected in this work. Similar assumptions have also been made in earlier works.[13,14] This leads to constant λ_m and D_p and correspondingly wave propagation becomes invariant of temperature distribution within the material.

Propagating microwave induces oscillating electric field within oil, which is dissipated as heat due to interactions with dipoles. In other words, microwave power is absorbed during propagation through oil and generated internal heat sources. The internal heat source is directly proportional to the absolute magnitude of induced electric field as given below:

$$Q(Z) = \pi f \epsilon_0 \kappa_m'' |E_X(Z)|^2, \tag{12}$$

where $E_X(Z)$ is the induced electric field within oil and $|E_X(Z)| = \sqrt{E_X(Z)E_X^*(Z)}$ with $E_X^*(Z)$ being complex conjugate of $E_X(Z)$. The determination of $E_X(Z)$ involves the solution of Helmholtz equations within oil and surrounding free spaces as discussed in details in the literature.[19,20] Here we only present the solution for clarity of discussion. The readers are referred to the above references for detail description.

The Helmholtz equations can be solved analytically for constant dielectric properties,[19,20] which can be substituted in Eq. (12) to obtain the following closed form expression for absorbed power distribution in terms of dimensionless coordinate z:

$$Q(z) = \frac{8\lambda_m I_0}{\lambda_0 D_p C_d}[C_{n,1}\cosh 2N_p z + C_{n,2}\sinh 2N_p z + C_{n,3}\cos 4\pi N_w z + C_{n,4}\sin 4\pi N_w z], \quad (13)$$

where

$$C_{n,1} = c_2\cosh N_p + c_4\sinh N_p + 2\sqrt{\phi_0(1-\phi_0)} \times (c_1\cos 2\pi N_w + c_3\sin 2\pi N_w), \quad (14a)$$

$$C_{n,2} = (1-2\phi_0)(c_2\sinh N_p + c_4\cosh N_p), \quad (14b)$$

$$C_{n,3} = c_1\cos 2\pi N_w + c_3\sin 2\pi N_w + 2\sqrt{\phi_0(1-\phi_0)} \times (c_2\cosh N_p + c_4\sinh N_p), \quad (14c)$$

$$C_{n,4} = -(1-2\phi_0)(c_1\sin 2\pi N_w - c_3\cos 2\pi N_w), \quad (14d)$$

$$C_d = (c_3^2 - c_1^2)\cos 4\pi N_w + (c_2^2 + c_4^2)\cosh 2N_p - 2c_1c_3\sin 4\pi N_w + 2c_2c_4\sinh 2N_p. \quad (14e)$$

In the above equations, the dimensionless parameters $N_w = L/\lambda_m$ and $N_p = L/D_p$ are called as wave number and penetration number, respectively, and $\phi_0 = I_B/I_0$ is the fractional incidence from bottom, where $I_0 = I_B + I_T$ is the total incident flux and I_T and I_B are incident fluxes from top and bottom, respectively. The dimensionless coefficients $c_1 - c_4$ are given by

$$c_1 = 1 + \frac{\lambda_m^2}{4\pi^2 D_p^2} - \frac{\lambda_m^2}{\lambda_0^2} = 0.644, \quad (15a)$$

$$c_2 = 1 + \frac{\lambda_m^2}{4\pi^2 D_p^2} + \frac{\lambda_m^2}{\lambda_0^2} = 1.358, \quad (15b)$$

$$c_3 = -\frac{\lambda_m^2}{\pi\lambda_0 D_p} = -0.032, \quad (15c)$$

$$c_4 = \frac{2\lambda_m}{\lambda_0} = 1.1948, \quad (15d)$$

where $\lambda_0 = 1/f\sqrt{\mu_0\epsilon_0} = 12.24$ cm is the wavelength within free space.

Substituting Eq. (13) in Eq. (3b) and integrating with respect to z using the boundary conditions [Eq. (4)], the microwave induced dimensionless base state temperature profile within oil can be expressed as

$$\theta_s(z) = \frac{1}{2} - z - \frac{8\lambda_m}{D_p C_d \Lambda}\left[\frac{C_{n,1}}{4N_p^2}(\cosh 2N_p z - \cosh N_p) + \frac{C_{n,2}}{4N_p^2}(\sinh 2N_p z - 2z\sinh N_p) + \frac{C_{n,3}}{16\pi^2 N_w^2}(\cos 2\pi N_w - \cos 4\pi N_w z) + \frac{C_{n,4}}{16\pi^2 N_w^2}(2z\sin 2\pi N_w - \sin 4\pi N_w z)\right], \quad (16a)$$

with

$$\Delta T_s = \frac{L^2 I_0}{\gamma\lambda_0}\Lambda, \quad (16b)$$

where

$$\Lambda = \frac{q_{av}}{2} + \frac{8\lambda_m}{D_p C_d}\left[\frac{C_{n,4}}{4\pi N_w}\left(\cos 2\pi N_w - \frac{\sin 2\pi N_w}{2\pi N_w}\right) + \frac{C_{n,2}}{2N_p}\left(\frac{\sinh N_p}{N_p} - \cosh N_p\right)\right]. \quad (16c)$$

In Eq. (16c), q_{av} is the dimensionless average power within oil layer defined as

$$q_{av} = \frac{\lambda_0}{I_0}\int_{-1/2}^{1/2} Q(z)dz. \quad (17)$$

Using Eq. (13), q_{av} can be written as

$$q_{av} = \frac{8\lambda_m}{D_p C_d}\left[\frac{C_{n,1}}{N_p}\sinh N_p + \frac{C_{n,3}}{2\pi N_w}\sin 2\pi N_w\right]. \quad (18)$$

The expression for $d\theta_s/dz$ for microwave induced heating is obtained from Eq. (16a) as

$$\frac{d\theta_s}{dz} = -1 - \frac{8\lambda_m}{D_p C_d \Lambda}\left[\frac{C_{n,1}\sinh 2N_p z + C_{n,2}\cosh 2N_p z}{2N_p} + \frac{C_{n,3}\sin 4\pi N_w z - C_{n,4}\cos 4\pi N_w z}{4\pi N_w} + \frac{C_{n,4}}{8\pi^2 N_w^2}\sin 2\pi N_w - \frac{C_{n,2}}{2N_p^2}\sinh N_p\right]. \quad (19)$$

III. NUMERICAL SCHEME AND VALIDATION

Equations (9) and (10) form a coupled eigenvalue problem with $\bar{\theta}$ and $\bar{w}$ being the eigenfunctions and Ra being the eigenvalue. Determination of onset of convection is equivalent to performing neutral stability analysis of Eq. (9), i.e., determination of first eigenvalue (Ra) as a function of k with $\sigma = 0$ and finding the minima of the function $\mathrm{Ra}(k)$ for various microwave related parameters. The minimum of Ra is called critical Rayleigh number (Ra_c) and the corresponding k is called critical wave number (k_c). Here, Galerkin weighted residual method has been used to determine the Ra_c and k_c, where $\bar{w}$ and $\bar{\theta}$ are expressed as

$$\bar{w}(z) = \sum_{i=0}^{n_\phi} w_i \phi_i(z) \quad \text{and} \quad \bar{\theta}(z) = \sum_{j=0}^{n_\psi} \theta_j \psi_j(z), \quad -1/2 \leqslant z \leqslant 1/2, \tag{20}$$

where $\phi_i(z)$ and $\psi_j(z)$ are basis functions associated with $\bar{w}$ and $\bar{\theta}$, respectively. The basis functions satisfy the corresponding boundary conditions given by

$$\phi_i = \frac{d\phi_i}{dz} = 0 \quad \text{at } z = \pm 1/2 \quad \text{and} \quad \begin{cases} \dfrac{d\psi_j}{dz} = 0 & \text{at } z = -1/2 \\ \psi_j = 0 & \text{at } z = 1/2. \end{cases} \tag{21}$$

Using Eq. (20), Eq. (9) can be transformed into the following discrete vector-matrix equation:

$$\mathbf{A_w w} = -\,\mathrm{Ra}\, \mathbf{B}_\theta \mathbf{A}_\theta^{-1} \mathbf{B_w w}, \tag{22}$$

where $w=[w_1 w_2 \cdots w_{n_\phi}]^T$ and

$$\left.\begin{aligned} A_w(k,i) &= \int_{-1/2}^{1/2} \left(\frac{d^2\phi_i}{dz^2}\frac{d^2\phi_k}{dz^2} + 2k^2 \frac{d\phi_i}{dz}\frac{d\phi_k}{dz} + k^4 \phi_i \phi_k \right) dz \\ A_\theta(l,j) &= \int_{-1/2}^{1/2} \left(\frac{d\psi_j}{dz}\frac{d\psi_l}{dz} - k^2 \psi_j \psi_l \right) dz \\ B_w(l,i) &= \int_{-1/2}^{1/2} \frac{d\theta_s}{dz} \phi_i \psi_l dz, \quad B_\theta(k,j) = k^2 \int_{-1/2}^{1/2} \psi_j \phi_k dz \end{aligned}\right\} \quad \begin{aligned} &j,l = 0,1,2,\ldots,n_\psi \\ &i,k = 0,1,2,\ldots,n_\phi. \end{aligned} \tag{23}$$

Equation (23) with corresponding $d\theta_s/dz$ is numerically solved using QZ algorithm[46] with the following basis functions:

$$\{\phi_i(z)\}_{i=0}^{n_\phi} = [1-(2z)^2]^2 T_i(z), \tag{24a}$$

$$\{\psi_j(z)\}_{i=0}^{n_\psi} = (2z+3)(2z-1)\left[T_j(z) + \frac{j^2}{(j+1)^2} T_{j+1}(z) \right], \tag{24b}$$

where $\{T_n(z)\}_{n=0}^{\infty} = \cos[n \cos^{-1}(2z)]$ is the Chebyshev polynomial. It may be noted that basis recombination technique as suggested by Heinrichs[47–49] has been used to find the present set of basis functions [Eq. (24)] from the Chebyshev polynomial. The derived basis functions not only satisfy the corresponding boundary conditions [Eq. (21)] but also reduce the condition number of the resultant matrix compared to the Chebyshev polynomial.

The numerical scheme is validated with uniform internal heat source for which $d\theta_s/dz = -(2z+1)$. Using $n_\phi = n_\psi = 10$, critical numbers are obtained as $k_c = 2.6295$ and $\mathrm{Ra}_c = 1386.137\,13$, which are in well agreement with those obtained by Robert[30] ($k_c = 2.629$ and $\mathrm{Ra}_c = 1386.14$). In order to conform the adequacy of number of basis function, n_ϕ and n_ψ are increased from 10 to 15 and the results are compared. It has been observed that k_c does not change with increasing number of basis function and Ra_c changes in fifth decimal place ($\mathrm{Ra}_c = 1386.137\,13$, $1386.137\,15$, and $1386.137\,15$ for $n_\phi = n_\psi = 10$, 11, and 15, respectively). Hence, $n_\phi = n_\psi = 10$ has been used in this work.

IV. ILLUSTRATIONS

A. Spatial patterns of $Q(z)$ and corresponding $\theta_s(z)$

It may be noted from Eqs. (13) and (16a) that $Q(z)$ and $\theta_s(z)$ are parametric functions of N_w, N_p, and ϕ_0. It may be further noted that $N_p = N_w \lambda_m / D_p \approx 0.17 N_w$ for oil. Thus, absorbed power and base state temperature profiles within oil are function of two independent parameters, namely, ϕ_0 and either of N_w or N_p. It is evident from the definitions that N_w and N_p simulate the effect of oil thickness on $Q(z)$ and $\theta_s(z)$ and vary between 0 and ∞ signifying transition from thin to thick oil layers, respectively. On the other hand, ϕ_0 captures the effect of distribution of microwave incidence (I_0) between top (I_T) and bottom (I_B) with constant total incident flux (I_0). It may be noted that $\phi_0 = 0$ and 1 represent one sided incidence (from top and bottom, respectively) and $\phi_0 = 1/2$ represents equal incidence from top and bottom. All other ϕ_0 corresponds to uneven distribution of microwave sources, where microwave incidence is stronger either from bottom for $\phi_0 > 1/2$ or from top for $\phi_0 < 1/2$. Thus, entire spectrum of microwave source configurations can be mimicked by varying ϕ_0 from 0 to 1.

Figure 2 illustrates spatial patterns of dimensionless absorbed power (scaled with I_0/λ_0) distributions and corresponding dimensionless base state profiles [$\theta_s(z)$] within oil of various thicknesses corresponding to $N_w = 0.05$ (0.366 cm), 0.1 (0.73 cm), 0.5 (3.66 cm), 1 (7.31 cm), and $N_p = 3$ (1.3 m), 6 (2.61 m). In Fig. 2, $q(z) \equiv Q(z)\lambda_0/I_0$ and $\theta_s(z)$ are shown for various microwave source configurations corresponding to $\phi_0 = 0$, 0.25, 0.5, 0.75, and 1. One important feature of absorbed power distribution may be observed from Fig. 2 as $q(z)|_{\phi_0} = q(-z)|_{1-\phi_0}$, i.e., absorbed power distribu-

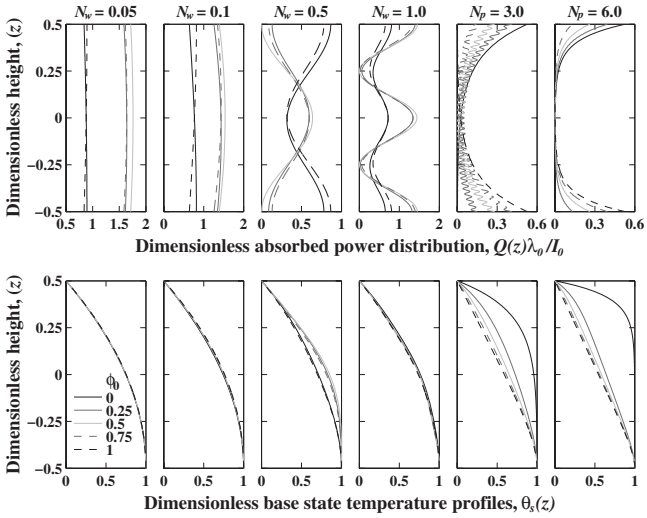

FIG. 2. Top panel shows the spatial patterns of dimensionless absorbed power, $Q(z)\lambda_0/I_0$, in thin (N_w=0.05,0.1), sinusoidal (N_w=0.5,1), and thick (N_p=3,6) sample regimes. Corresponding base state dimensionless temperature profiles [$\theta_s(z)$] are shown at the bottom panel.

tions corresponding to $\phi_0=j$ and $\phi_0=1-j$ are mirror reflections of each other around the horizontal plane at $z=0$. This leads to the fact that absorbed power distributions are symmetric around the center for $\phi_0=1/2$, as may be seen from Fig. 2.

It may be observed from Fig. 2 that $q(z)$ exhibits three distinct spatial distributions, namely (i) uniform, (ii) sinusoidal, and (iii) exponential, as oil thickness increases from 0.366 cm to 2.61 m. This is due to the fact that Eq. (13) contains both exponential (hyperbolic functions) and sinusoidal position dependencies, where the coefficients $C_{n,1}-C_{n,4}$ determine the relative contribution of these terms in determining the spatial patterns of absorbed power distributions. Since $C_{n,1}-C_{n,4}$ depend on N_w, N_p, and ϕ_0 [see Eqs. (14a)–(14d)], relative contributions of exponential terms compared to sinusoidal terms vary with varying oil thickness and microwave source configurations generating various spatial patterns of $q(z)$ shown in Fig. 2. However, the position dependencies of $q(z)$ disappear if the oil thickness is much less than that required to complete a cycle of sinusoidal functions of Eq. (13). This regime of oil samples is referred as *thin* samples. An analysis of the sinusoidal functions of Eq. (13) reveals that the criterion for attaining thin sample regime is given by $N_w \ll 0.5$. In thin oil samples, microwave is absorbed uniformly irrespective of ϕ_0 and correspondingly $\theta_s(z)=3/4-z-z^2$ becomes invariant of microwave source configurations, as shown in Fig. 2 for N_w=0.05 and 0.1.

Nonuniform spatial patterns of absorbed power gradually evolve as oil thickness increases beyond thin sample regime, where $q(z)$ follows either sinusoidal or exponential function of Eq. (13). The sinusoidal patterns appear for $N_p \not\gg 1$, while exponential distributions of absorbed power are obtained for $N_p \gg 1$. The former will be referred as *sinusoidal* regime and the later will be called as *thick* sample regime. The spatial oscillations of $q(z)$ in sinusoidal regime are characterized by N_w, whereas exponential regime is characterized by N_p. It may be interesting to note that the critical oil thickness required to reach the exponential regime depends on microwave source configurations. Absorbed power reaches exponential distributions in thinner oil layers ($N_p \geqslant 3$) for one sided incidence than that required for distributed incidence ($N_p \geqslant 6$), as may be seen from Fig. 2. It may be noted that spatial nonuniformity of $q(z)$ results in intensification of absorbed power at either top or bottom of the oil based on ϕ_0 in both exponential and sinusoidal regimes. It may be further noted that absorbed power intensifies toward the stronger microwave source in exponential regime. On the other hand, $q(z)$ may intensify either towards or opposite to the stronger microwave source depending on N_w in sinusoidal regime. This results in strong dependence of base state temperature profiles on N_w in the sinusoidal regime, as may be seen from Fig. 2.

In sinusoidal regime, the absorbed power profiles for various microwave source configurations may or may not be in the same phase state and correspondingly, $\theta_s(z)$ shows either weak or strong dependence on ϕ_0, respectively. For example, $q(z)$ corresponding to one sided incidence (ϕ_0=0 and 1) are in opposite phase state with those corresponding to distributed microwave incidence (ϕ_0=0.25, 0.5, and 0.75) for N_w=0.5. On the other hand, the absorbed power distributions remain in the same phase state for all microwave source configurations for N_w=1. Accordingly, $\theta_s(z)$ exhibits stronger dependence on θ_0 for N_w=0.5 compared to N_w=1. It may be further noted that distributed microwave incidence results in stronger quasistable temperature layer at the bottom of the oil compared to one sided incidence for N_w=0.5. Within the quasistable layer, the temperature remain almost constant at θ_s=1. The formation of quasistable temperature layer, which prohibits the onset on convection, depends on ϕ_0 and N_w in the sinusoidal regime. On the other hand, quasistable layer is formed irrespective of N_p in exponential regime if microwave incidence is mainly focused from top.

In the exponential regime, microwave power is absorbed from the surfaces and penetrates inside the oil, as can be seen from Fig. 2 for N_p=3 and N_p=6. This leads to the situation of surface heating in the limit of $N_p \to \infty$, where surface heat sources at top and bottom surfaces are proportional to $1-\phi_0$ and ϕ_0, respectively. Thus, any nonzero ϕ_0 resembles the situation of surface heating from bottom in the limit of $N_p \to \infty$ and correspondingly base state temperature asymptotically approaches the associated linear profile $\theta_s(z)=1/2-z$ as oil thickness increases in exponential regime. This can be seen from Fig. 2 for ϕ_0=1, 0.75, 0.5, and 0.25. On the other other, a strong quasistable temperature layer is formed at the bottom of oil in exponential regime for ϕ_0=0, where heating is entirely from top. It may be noted that the height of quasistable layer increases as N_p increases in exponential regime and almost entire oil layer remains at θ_s=1 in the limit of $N_p \to \infty$.

B. Average absorbed power and ΔT_s

Figure 3 illustrates the variations of dimensionless average absorbed power (q_{av} in subplot a) and dimensionless base state temperature difference between top and bottom surface ($\overline{\Delta T_s}=\gamma\lambda_0\Delta T_s/L^2I_0 \equiv \Lambda$ in subplot b) with oil thickness varying from thin ($N_w=10^{-2}$) to thick ($N_w=10^2$) sample

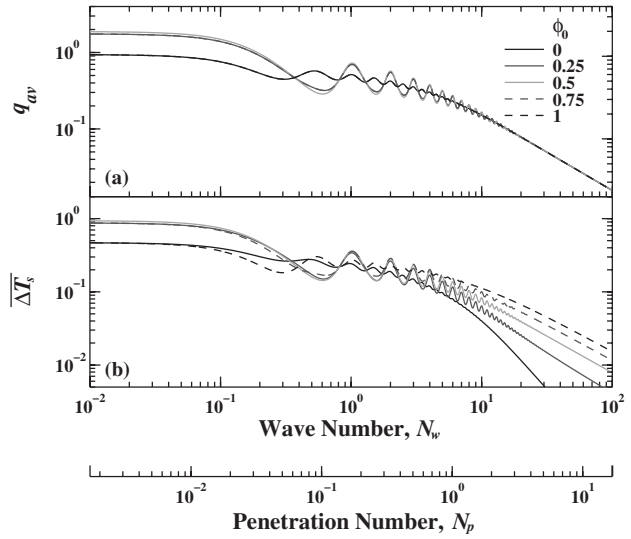

FIG. 3. Variations of dimensionless average absorbed power [q_{av} in subplot (a)] and dimensionless base state temperature difference between top and bottom plates [$\overline{\Delta T_s}$ in subplot (b)] from thin to thick sample regimes. The results are shown for various representative microwave source configurations as $\phi_0=0$, 0.25, 0.5, 0.75, and 1.

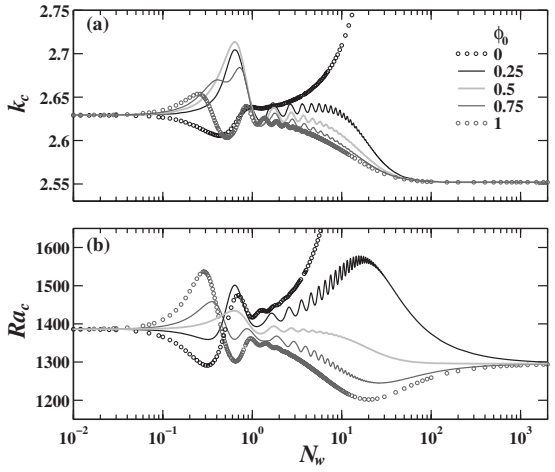

FIG. 4. Variations of k_c [subplot (a)] and Ra_c [subplot (b)] from thin to thick sample regimes for various microwave source configurations as $\phi_0=0$, 0.25, 0.5, 0.75, and 1.

regimes. The corresponding penetration numbers ($N_p=0.0017$ to $N_p=16.82$) are shown at the bottom of the plot. It may be noted that $\overline{\Delta T_s}$ represents the maximum temperature difference within oil layer at base state. In Fig. 3, the variations of q_{av} and $\overline{\Delta T_s}$ are shown for various microwave source configurations as $\phi_0=0$, 0.25, 0.5, 0.75, and 1. Here, q_{av} for various N_w and ϕ_0 is determined from Eq. (18) and $\overline{\Delta T_s}$ has been determined from Eq. (16c). It may be noted from Fig. 3(a) that average power is invariant of the orientation of microwave source, i.e., $q_{\mathrm{av}}|_{\phi_0=0}=q_{\mathrm{av}}|_{\phi_0=1}$ and $q_{\mathrm{av}}|_{\phi_0=0.25}=q_{\mathrm{av}}|_{\phi_0=0.75}$.

It is interesting to note that similar to $q(z)$, both q_{av} and $\overline{\Delta T_s}$ exhibit three distinct behaviors corresponding to (i) thin, (ii) sinusoidal, and (iii) thick samples. For thin samples, Eq. (16b) can be simplified to

$$\lim_{N_w \ll 0.5} \overline{\Delta T_s} = \frac{q_{\mathrm{av}}}{2} = \frac{\lambda_0^2}{D_p \lambda_m}(1+2\sqrt{\phi_0(1-\phi_0)})\left[1-\frac{2\lambda_0}{D_p}N_w\right]. \tag{25}$$

Thus, $\overline{\Delta T_s}$ follows q_{av} in the thin sample regime, where distributed microwave incidence results in higher power absorption compared to one sided incidence. Correspondingly, $\overline{\Delta T_s}$ is higher for $\phi_0=1/2$ than for $\phi_0=0$ or 1 in thin oil samples as may be observed from Fig. 3. It may also be noted that imposed temperature difference at base state is invariant of the orientation of microwave source in thin sample regime such that $\overline{\Delta T_s}(\phi_0)=\overline{\Delta T_s}(1-\phi_0)$. On the other hand, $\overline{\Delta T_s}$ depends on the orientation of microwave source in thick samples, where Eq. (16b) can be reduced to be

$$\lim_{N_p \gg 1} \overline{\Delta T_s} = \frac{2\lambda_m}{D_p N_p (c_2+c_4)}\left[1+(1-2\phi_0)\left(\frac{1}{N_p}-1\right)\right]. \tag{26}$$

In this regime, the absorbed power becomes invariant of ϕ_0 given by $q_{\mathrm{av}}=4\lambda_m/D_pN_p(c_2+c_4)$. However, $\overline{\Delta T_s}$ depends strongly on ϕ_0, as shown in Fig. 3. In thick oil samples, the imposed temperature difference decreases as microwave source is oriented towards top, i.e., ϕ_0 decreases from 1 to 0. In contrast, $\overline{\Delta T_s}$ may be enhanced by either one sided or distributed incidence in sinusoidal regime. In sinusoidal regime, both q_{av} and $\overline{\Delta T_s}$ oscillate with oil thickness and exhibit maxima at $N_w=j/2$ for one sided incidence and at $N_w=j$ for distributed incidence. In this regime, distributed incidence impose greater temperature difference at $N_w=j$ for moderate N_w. On the other hand, one sided incidence cause greater $\overline{\Delta T_s}$ at $N_w=j/2$ for N_w well below the thick sample regime.

V. CRITICAL RAYLEIGH NUMBER AND WAVE NUMBER

It is evident from previous discussions that absorbed power and corresponding base state temperature profiles exhibit a wide spectrum of nonlinear patterns as oil thickness (equivalently N_w or N_p) varies from thin to thick sample regimes. As a result, critical Rayleigh and wave numbers also exhibit highly nonlinear variations from thin to thick sample regimes corresponding to various patterns of $Q(z)$, as shown in Fig. 4. In this figure, variations of k_c (subplot a) and Ra_c (subplot b) are shown as function of N_w for various microwave source configurations as $\phi_0=0$, 0.25, 0.5, 0.75, and 1.

It may be observed from Fig. 4 that both k_c and Ra_c exhibit three distinct regimes corresponding to thin, sinusoidal, and thick samples. In the thin sample regime, critical Rayleigh and wave numbers asymptotically reach thin sample asymptotes invariant of ϕ_0. On the other hand, the variations of critical Rayleigh and wave numbers in thick sample regime depend on whether $\phi_0=0$ or $\phi_0\neq 0$. It may be noted that Ra_c and k_c attain the thick sample asymptote if $\phi_0\neq 0$ but increases exponentially with N_w in the thick sample regime if $\phi_0=0$. In between thin and thick sample asymptotes, both Ra_c and k_c oscillate with N_w following the oscillatory behavior of absorbed power. In this regime, the amplitude and the width of the oscillatory regime depends on

the microwave source configurations, where unevenly distributed microwave incidence ($\phi_0=0.25$ and 0.75) cause higher and wider oscillations than either one sided ($\phi_0=0$ and 1) or equally distributed ($\phi_0=1/2$) microwave incidence.

The critical wave and Rayleigh numbers in Fig. 4 are determined from Eq. (9) by evaluating $d\theta_s/dz$ from Eq. (19) and finding the minimum Rayleigh number and corresponding wave number for various N_w and ϕ_0 following the procedure described in Sec. III. Thus, Ra_c is a parametric function of $d\theta_s/dz$, which depends on the spatial patterns of θ_s. The spatial patterns of $\theta_s(z)$ in turn are function of N_w and ϕ_0, as discussed in Sec. II A. However, normalized base state temperature $[\theta_s(z)]$ does not depend on the absolute magnitude of absorbed power ($|Q(z)|$) and varies between 0 and 1 due to scaling with respect to ΔT_s, which takes into account the magnitude of imposed temperature field at base state. As a result, critical Rayleigh number based on present definition depends only on the spatial pattern of $Q(z)$ via $d\theta_s/dz$ and does not depend on $|Q(z)|$.

The above fact is manifested in thin sample asymptotes of Ra_c and k_c as they become invariant of the microwave source configurations in spite of the fact that $|Q(z)|$ differs significantly from one side incidence to distributed incidence. This is due to the fact that microwave is absorbed uniformly in thin enough oil samples, which results in $Q(z)/|Q(z)|=1$ and $\theta_s(z)=3/4-z-z^2$ irrespective of N_w and ϕ_0 (see Fig. 2). Consequently, critical Rayleigh and wave numbers asymptotically attain the thin sample asymptotes corresponding to uniform internal heat source given by $\mathrm{Ra}_c^0=1386.137\,15$ and $k_c^0=2.6295$. Similarly, microwave power absorption patterns in thick oil samples resemble the surface heating from bottom for $\phi_0\neq 0$ and $\theta_s=1/2-z$ is attained in thick enough samples irrespective of N_w and ϕ_0 $\forall\phi_0\neq 0$. Correspondingly, critical Rayleigh and wave numbers attain thick sample asymptotes associated with bottom heating given by $\mathrm{Ra}_c^\infty=1295.7779$ and $k_c^\infty=2.552$ although the strength of bottom heat source varies in proportion with ϕ_0. On the other hand, microwave power absorption occurs only from top surface for $\phi_0=0$ and tends to the surface heat source from top in the limit of $N_w\to\infty$. Thus, onset of convection is prohibited with increasing oil thickness in the thick sample regime if microwave incidence is solely from top ($\phi_0=0$) and consequently Ra_c and k_c shoots up exponentially for as oil thickness increases in thick sample regime.

An interesting fact becomes evident from the above discussion that spatial profiles of microwave power absorption have direct consequence on critical Rayleigh and wave numbers. This can be further seen from Fig. 4(b) as the variations of Ra_c with N_w for $\phi_0=j$ are almost mirror reflections of those for $\phi_0=1-j$. Similar qualitative trends are also observed in absorbed power distributions, as discussed in Sec. II A. It may be noted that every maxima of Ra_c in sinusoidal regime for $\phi_0=0$ and 0.25 correspond to a minima of Ra_c for $\phi_0=1$ and 0.75, respectively. On the other hand, the variations of k_c with N_w follow almost similar pattens for various microwave source configurations except $\phi_0=0$. It may be noted that critical wave number reaches the lowest value in thick oil samples ($k_c^\infty=2.552$) and the transition to k_c^∞ exhibit an overall decrease for $\forall\phi_0\neq 0$ (Fig. 4). In contrast, the critical Rayleigh number for $\phi_0>1/2$ attain a much lower value than Ra_c^∞ prior to the thick sample asymptote and the transition to the thick sample asymptote occurs via a global minima as can be seen from Fig. 4(b). Similarly, the transition from sinusoidal regime to Ra_c^∞ exhibit a global maxima for $\phi_0<1/2$. These distinguishing features of critical Rayleigh and wave numbers are due to the fact that Ra_c represents the probability of the onset of convection, while k_c is a measure of the size of the convection cell at the onset. Although Ra_c and k_c characterize two different aspects of onset of convection, they are the manifestation of the absorbed power distribution profiles. Thus, variation patterns of Ra_c and k_c from thin to thick sample regimes can be correlated to the qualitative trends of absorbed power distributions as will be discussed below in details.

A. Role of $Q(z)$ on variations of Ra_c with N_w and ϕ_0

It is physically intuitive that onset of convection during microwave heating is facilitated if absorbed power is intensified more at the bottom. Thus, the probability of occurrence of onset may be related to the relative power intensification in the bottom half of the oil compared to the top half. Let us define δ_{bottom} as

$$\delta_{\mathrm{bottom}}=\frac{\int_{z=-1/2}^{0}Q(z)dz}{\int_{z=-1/2}^{1/2}Q(z)dz}=\frac{1}{2}-\frac{2\pi N_w C_{n,2}\sinh^2\frac{N_p}{2}+N_p C_{n,4}\sin^2\pi N_w}{2\pi N_w C_{n,1}\sinh N_p+N_p C_{n,3}\sin 2\pi N_w},\qquad(27)$$

where δ_{bottom} represents the fractional power absorption in the bottom half of oil. It may be noted that $\delta_{\mathrm{bottom}}=0$ implies no power absorption in the bottom half, while $\delta_{\mathrm{bottom}}=1$ indicate entire power absorption in the bottom half of the sample. Thus, the intensification of absorbed power shifts toward bottom of oil with increasing δ_{bottom}, which facilitates the onset of convection. This is indicated as decreasing trends of Ra_c as lower critical Rayleigh number represents easier onset of convection. Similarly, higher prediction of Ra_c can be related to lower δ_{bottom}. Thus, the variations of critical Rayleigh number from thin to thick oil samples for various ϕ_0 can be inversely correlated to δ_{bottom}, as shown in Figs. 5(a)–5(d) for $\phi_0\neq 1/2$.

It may be noted that $\delta_{\mathrm{bottom}}\neq 1/2$ indicates asymmetric power absorption around the center and variations of δ_{bottom} with N_w occurs not only due to change of extent of asymmetry but also due to relocation of the absorbed power intensification within the domain. Thus, δ_{bottom} remains constant at $1/2$ for $\phi_0=1/2$, where symmetric power distributions around the center are attained irrespective of N_w. In this case, variations of Ra_c with N_w can be related to the change on relative power absorption near the bottom surface. Here, we consider lower 25% of the domain and define

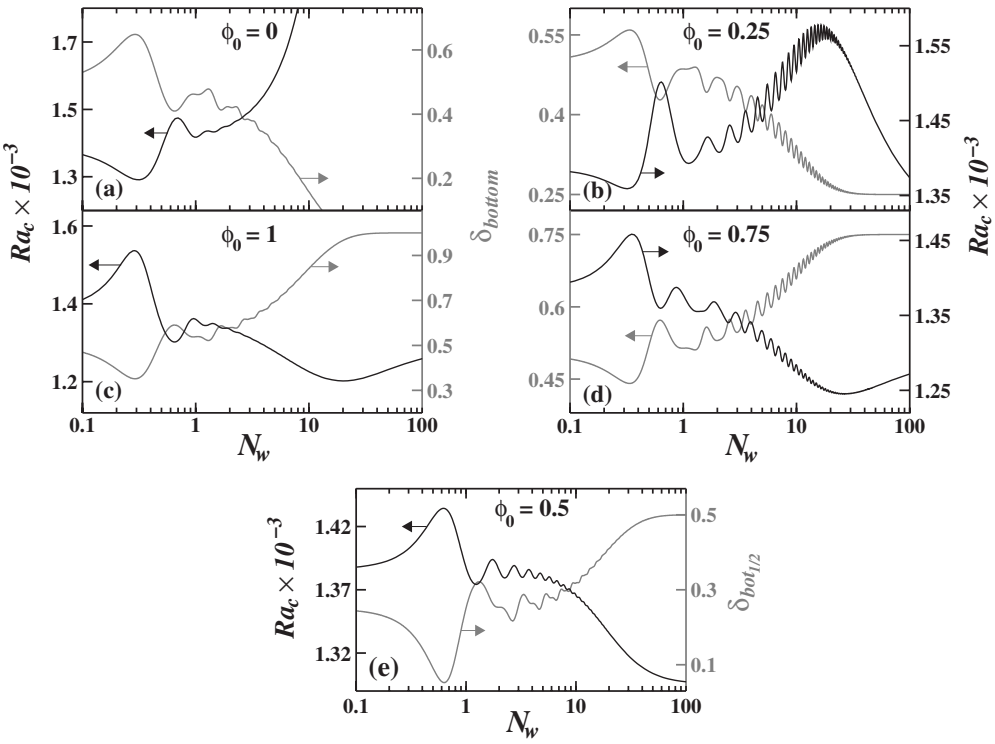

FIG. 5. Comparisons between the variations of Ra_c and δ_{bottom} for $\phi_0 \neq 1/2$ [subplots (a)–(d)] or $\delta_{\mathrm{bot}_{1/2}}$ for $\phi_0 = 1/2$ [subplot (e)] from thin to thick samples.

$$\delta_{\mathrm{bot}_{1/2}} = \frac{\int_{z=-1/2}^{-1/4} Q(z)dz}{\int_{z=-1/2}^{1/2} Q(z)dz},$$

$$= \frac{1}{2} - \left[2\pi N_w \left(C_{n,1} \cosh \frac{N_p}{4} + C_{n,2} \sinh \frac{3N_p}{4} \right) \sinh \frac{N_p}{4} + N_p \left(C_{n,3} \cos \frac{\pi N_w}{2} + C_{n,4} \sin \frac{3\pi N_w}{2} \right) \sin \frac{\pi N_w}{2} \right] \Bigg/ \left[2\pi N_w C_{n,1} \sinh N_p + N_p C_{n,3} \sin 2\pi N_w \right]. \quad (28)$$

The variations of $\delta_{\mathrm{bot}_{1/2}}$ and Ra_c for $\phi_0 = 1/2$ are shown in Fig. 5(e) over the entire range of N_w from thin to thick samples.

Figure 5 illustrate that the variation patterns of Ra_c with N_w are inversely replicated in corresponding δ_{bottom} [for $\phi_0 \neq 1/2$ in Figs. 5(a)–5(d)] and in $\delta_{\mathrm{bot}_{1/2}}$ [for $\phi_0 = 1/2$ in Fig. 5(e)] curve. Similar to Ra_c, δ_{bottom}, and $\delta_{\mathrm{bot}_{1/2}}$ predict three distinct regimes associated with thin, sinusoidal and thick oil samples. Correspondingly, δ_{bottom} and $\delta_{\mathrm{bot}_{1/2}}$ attain thin ($\delta_{\mathrm{bottom}} \to 1/2$, $\delta_{\mathrm{bot}_{1/2}} \to 1/4$) and thick ($\delta_{\mathrm{bottom}} \to \phi_0$, $\delta_{\mathrm{bot}_{1/2}} \to \phi_0(1-e^{-N_p/2})$) sample asymptotes in accordance with critical Rayleigh number. In sinusoidal regime, δ_{bottom} oscillate with N_w signifying continuous relocation of absorbed power intensification with varying oil thickness. In this regime, each maxima of Ra_c corresponds to either a minima or a plateau in the corresponding δ_{bottom} or $\delta_{\mathrm{bot}_{1/2}}$. Similarly, every minima in Ra_c versus N_w curves can be associated with a maxima or a plateau in δ_{bottom} or $\delta_{\mathrm{bot}_{1/2}}$. It is interesting to note that not only the location but also the amplitudes of oscillation of Ra_c and δ_{bottom} or $\delta_{\mathrm{bot}_{1/2}}$ have one to one correspondence. Thus, the variation patterns of Ra_c from thin to thick sample regimes can be predicted from absorbed power distribution profiles.

B. Role of $Q(z)$ on variations of k_c with N_w and ϕ_0

As mentioned in Sec. V, inverse of wave number indicates the size of convection cell. The size of the convection cell is influenced by the location of the its origin. The largest convection cell occurs if it originates from the bottom surface, which is also evident from Fig. 4(a) as k_c reaches its lowest values for surface heating from bottom. The size of the convection cell decreases as the intensification of absorbed power moves away from the bottom surface. This is manifested as an increase in k_c. It may be noted that absorbed power near the top plate does not influence the size of convection if top surface is maintained at constant temperature. Thus, a measure may be defined to correlate $k_c(N_w, \phi_0)$ with $Q(z)$ as

$$\delta = \frac{\int_{z=-0.35}^{0.25} Q(z)dz}{\int_{z=-0.5}^{0.25} Q(z)dz} \equiv 1 - \frac{\int_{z=-0.5}^{-0.35} Q(z)dz}{\int_{z=-0.5}^{0.25} Q(z)dz}. \quad (29)$$

In Eq. (29), $1-\delta$ represents the relative power absorption within lower 15% of the domain compared to that within lower 75% of the domain.

It may be noted that increasing δ signifies smaller convection cell. This is due to the fact that increasing δ results in wider quasistable temperature layers due to upward shifting of intensification of absorbed power and moves up the origin of convection cell. Thus, critical wave number increases with increasing δ. Similarly, the size of convection cell increases as δ decreases, which results in decreasing k_c. Thus, k_c and δ follow the similar trends with N_w, as shown in Fig. 6, where

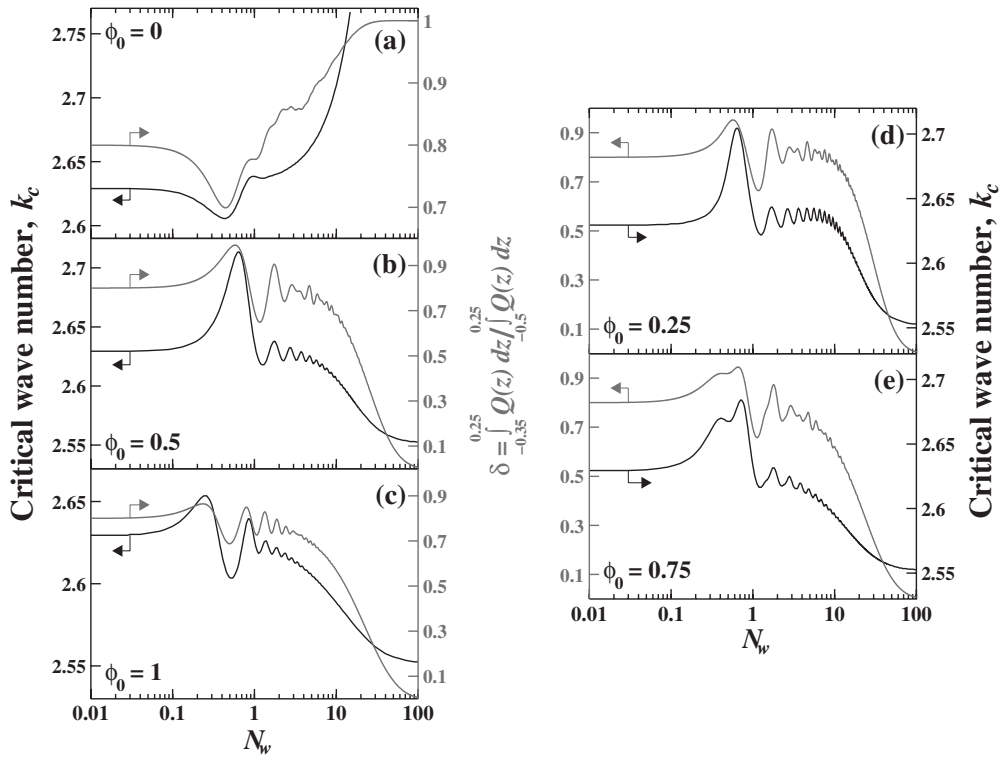

FIG. 6. Comparisons between the variations of k_c and δ from thin to thick samples for various microwave source configurations as ϕ_0=0 [subplot (a)], 0.25 [subplot (d)], 0.5 [subplot (b)], 0.75 [subplot (e)], and 1 [subplot (c)].

the variations of k_c and δ for various ϕ_0 are shown over the entire range of thin to thick oil samples. It may be observed from Fig. 6 that variation patterns of k_c and δ show one-to-one correspondence for all the microwave source configurations. Similar to k_c, δ also exhibit thin, sinusoidal, and thick sample regimes. In accordance with thin and thick sample asymptotes of k_c, δ attains 0.8 irrespective of microwave source configurations in thin oil samples, while δ approaches $(1-\phi_0+\phi_0 e^{0.2N_p})/(1-\phi_0+\phi_0 e^{0.5N_p})$ with increasing N_w in thick oil samples. Similarly, the variation patterns of k_c in sinusoidal regime can be traced from that of δ, where every maxima or minima of k_c and δ appear at same N_w. It may also be noted that the transition from thin to sinusoidal and sinusoidal to thick sample of k_c and δ occur at same N_w.

VI. MODIFIED RAYLEIGH NUMBER ($\overline{\text{RA}}_C$)

Using Eq. (16b), the definition of Rayleigh number can be rewritten as

$$\text{Ra} = \frac{L^5 g\beta I_0}{\gamma\nu_0\alpha_0\lambda_0}\Lambda, \tag{30}$$

where Λ considers the absorbed power distribution patterns within the domain. It may be noted that Λ is given by the thin sample asymptote [Eq. (25)] for uniform power absorption, while any other value of Λ signifies deviation of $Q(z)$ from uniform spatial distribution. Thus, the variations of Λ with oil thickness introduce additional factor to the incident microwave flux I_0 and the definition of Rayleigh number given in Eq. (30) does not reflect the total incident flux required to onset the convection. On the other hand, $\overline{\text{Ra}}=\text{Ra}/\Lambda=\text{Ra}/\Delta\bar{T}_s$ can be defined in order to evaluate the the variations total incident flux necessary for onset of convection with oil thickness.

The variations of $\overline{\text{Ra}}_c$ with N_w are shown in Fig. 7 for various microwave source configurations. It may be noted that total incident flux required for onset of convection is inversely proportional to imposed base state temperature difference between the top and bottom surface for the thermal boundary conditions given by Eq. (2). As a result, distributed microwave source configurations result in lower $\overline{\text{Ra}}_c$ for thin oil samples signifying the onset of convection at lower inci-

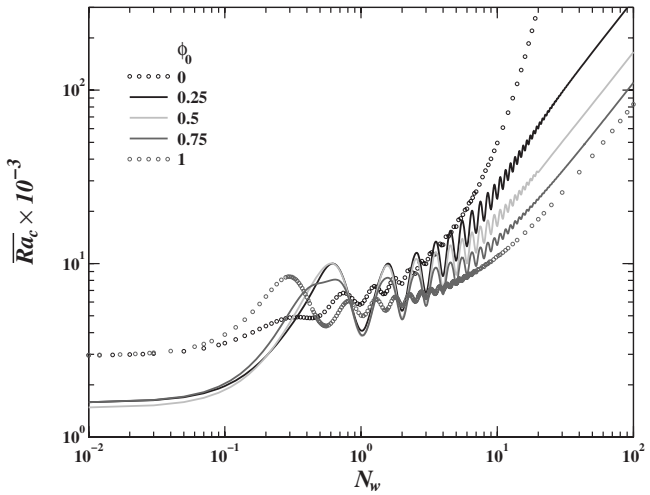

FIG. 7. Variations of modified critical Rayleigh number ($\overline{\text{Ra}}_c$) from thin to thick samples for various microwave source configurations as ϕ_0=0, 0.25, 0.5, 0.75, and 1.

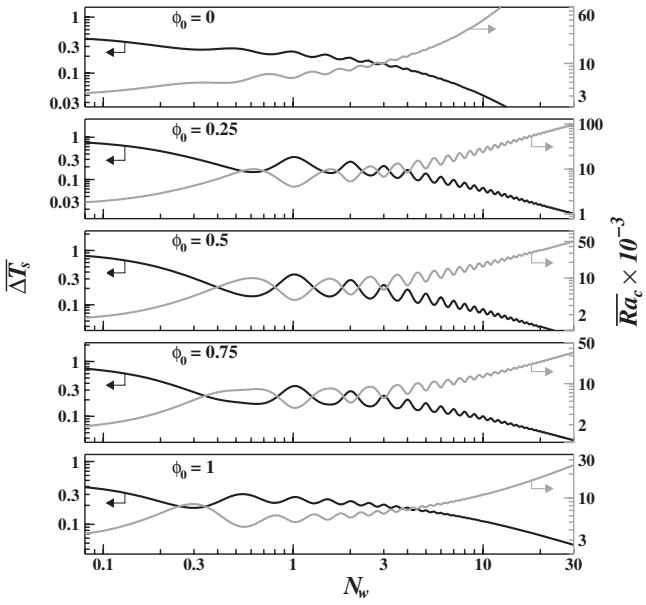

FIG. 8. Comparisons between the variations of modified Rayleigh number ($\overline{\mathrm{Ra}_c}$) and dimensionless temperature difference between top and bottom plates at conduction state ($\overline{\Delta T_s}$) from thin to thick samples for various microwave source configurations as ϕ_0=0, 0.25, 0.5, 0.75, and 1.

dent flux, as may be observed from Fig. 7. Also, $\overline{\mathrm{Ra}_c}$ does not depend on the orientation of microwave source in thin oil samples following ΔT_s (refer to Sec. IV B). In contrast, modified Rayleigh number ($\overline{\mathrm{Ra}_c}$) depends on the orientation of microwave source in thick oil samples (where $\Delta T_s \propto \phi_0$), as can be seen from Fig. 7. In thick oil samples, $\overline{\mathrm{Ra}_c}$ increases as microwave source moves away from the bottom (ϕ_0 reduces from 1 to 0). In sinusoidal regime, either one sided or distributed microwave incidence may lower $\overline{\mathrm{Ra}_c}$ depending on ΔT_s, which in turn depends on N_w. It may be seen from Fig. 7 that the transition of $\overline{\mathrm{Ra}_c}$ from sinusoidal to thick sample occurs at smaller N_w for one sided microwave incidence compared to distributed incidence, which are in accordance with ΔT_s. It may also be noted that distributed incidence results in much higher oscillations of $\overline{\mathrm{Ra}_c}$ following the similar behavior of ΔT_s (see Fig. 3).

It has already been mentioned that $\overline{\mathrm{Ra}_c}$ is inversely related to ΔT_s. Thus, the variations of $\overline{\mathrm{Ra}_c}$ from thin to thick samples especially in sinusoidal regime can be predicted from those of ΔT_s, as shown in Fig. 8 for various ϕ_0. Figure 8 illustrates that the variations of $\overline{\Delta T_s}$ can be used in order to forecast the variation patterns of $\overline{\mathrm{Ra}_c}$ in all the three regimes. In sinusoidal regime, peaks of $\overline{\mathrm{Ra}_c}$ appear at $N_w = j$ for distributed incidence (ϕ_0=0.25, 0.5, and 0.75) and at $N_w = j/2$ for one sided incidence (ϕ_0=0 and 1). Correspondingly, ΔT_s exhibit minima at those locations. Similarly, every local minima of $\overline{\mathrm{Ra}_c}$ in sinusoidal regime correspond to a maxima in ΔT_s. It may be interesting to note that not only the locations but also the amplitudes of oscillations correlate well for ΔT_s and $\overline{\mathrm{Ra}_c}$.

VII. CONCLUSIONS

The onset of natural convection during microwave heating of oil confined between two horizontal rigid plates has been analyzed for various oil thicknesses characterized by uniform (thin), sinusoidal (intermediate), and exponential (thick) power absorption. The analysis has been performed for various probable microwave source configurations ranging from one sided to distributed incidences of varying intensities from top and bottom. The critical Rayleigh (Ra_c) and wave (k_c) numbers have been determined by performing linear stability analysis of coupled momentum and energy balance equations in conjunction with Helmholtz equations. Helmholtz equations have been used to determine the spatial patterns of microwave induced heat source distributions within the sample, which vary with oil thickness and microwave source configurations. Thus, the base state temperature difference between top and bottom plates (ΔT_s) also vary with oil thickness and microwave source configurations (refer to Fig. 3) and complicates analysis of onset during microwave heating. Hence, we have used two different definitions for Rayleigh number, namely Rayleigh number ($\mathrm{Ra}_c = L^3 g \beta \Delta T_s / \nu_0 \alpha_0$) based on ΔT_s and modified Rayleigh number ($\overline{\mathrm{Ra}_c} = L^5 g \beta I_0 / \gamma \nu_0 \alpha_0 \lambda_0$) based on the incident intensity of microwave radiations (I_0), where Ra_c indicates the relative probability of onset and $\overline{\mathrm{Ra}_c}$ represents the incident microwave power required for the onset.

It has been observed that Ra_c is invariant of sample thickness and microwave source configurations in thin oil samples indicating equal possibility of onset of convection, while $\overline{\mathrm{Ra}_c}$ indicates that microwave power required to trigger the onset depend on microwave source configurations. In thin oil samples, distributed incidences require less microwave power and can be judiciously used to control the onset of convection. Similarly, thick sample asymptote of Ra_c indicates equal possibility of onset for all microwave source configurations except ϕ_0=0, which corresponds to microwave incidence solely from top. However, $\overline{\mathrm{Ra}_c}$ shows that incident microwave power required for the onset of convection in thick oil samples increases as microwave sources concentrates at the top. On the other hand, both Ra_c and $\overline{\mathrm{Ra}_c}$ indicate that it is almost impossible to induce convection in thick oil samples exposed to microwave from top (ϕ_0=0). Similarly, asymptotic behaviors of k_c indicate that the convection cell sizes are invariant of microwave source configurations in thin and thick oil samples.

In the intermediate regime, both Ra_c and $\overline{\mathrm{Ra}_c}$ are highly nonlinear functions of oil thickness and microwave source configurations and exhibit oscillations with oil thickness. The in-phase behavior of Ra_c with the degree of intensification of absorbed power at bottom of oil layer (δ_{bottom} or $\delta_{\mathrm{bot}_{1/2}}$) reveals the interesting physics underlying the possibility of onset of convection in the intermediate regime based on the stratification of quasistable base state temperature profiles. Similarly, the oscillatory variations of $\overline{\mathrm{Ra}_c}$ in the intermediate regime follow those of ΔT_s, which is physically intuitive. The oscillations of Rayleigh numbers in the intermediate regime show that onset of natural convection can be counterintuitively facilitated in thicker oil samples. In other words, the onset of convection can be controlled by selecting oil thickness or microwave source configurations based on Fig. 4 or 7. The critical wave number also exhibits oscillations in intermediate regime, which are in phase with δ, where $1-\delta$ represents the degree of intensification of absorbed power in

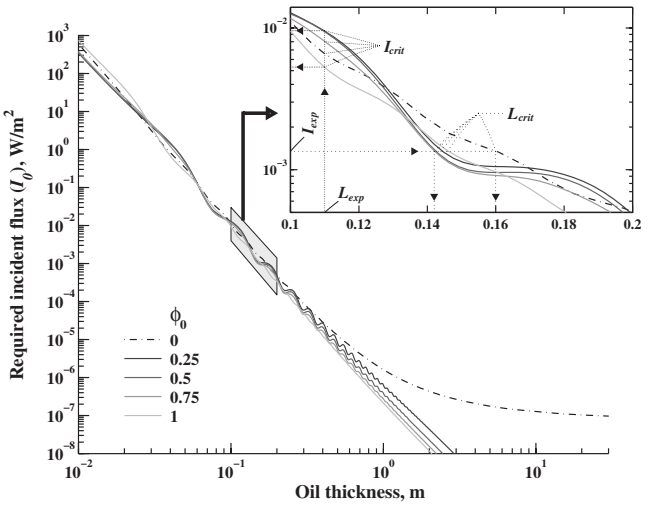

FIG. 9. Required total intensity of incident microwave radiations (I_0) for onset of convection within oil vs oil thickness for various microwave source configurations (ϕ_0=0, 0.25, 0.5, 0.75, and 1).

lower 15% of the domain. This implies that the size of the convection cell can be manipulated in a controlled way based on Fig. 4. Thus, Fig. 4 or 7 can be used as master curves to forecast the onset of convection and select the experimental parameters for onset of convection and associated cell size as illustrated below.

Figure 9 illustrates total incident flux (I_{crit}) required for the onset of convection within oil of varying thicknesses between 1 cm and 30 m. It may be noted that $I_{crit}=\overline{\mathrm{Ra}}_c\nu_0\alpha_0\gamma\lambda_0/g\beta L^5$ has been determined from the modified critical Raleigh number ($\overline{\mathrm{Ra}}_c$) obtained in Sec. VI using $\gamma=0.168$ W m^{-1} K^{-1}, $\beta=6.88\times10^{-4}$ K^{-1}, $\mu=0.05$ kg m^{-1} s^{-1}, $C_p=2000$ J kg^{-1} K^{-1}, $\rho_0=900$ kg m^{-3}, and $g=9.81$ m s^{-2}. Let us first fix the oil thickness at L_{exp} as shown in the inset plot. It is of practical importance to know the required total incident flux (I_{crit}) to initiate convection within specified oil thickness (L_{exp}), which can be obtained from Fig. 9 for various microwave source configurations, as highlighted via vertical and horizontal arrows in the inset plot. Thus, Fig. 9 can be used as master curve for determining I_{crit} for various oil thicknesses. It may be noted from Fig. 9 that for a fixed oil thickness, total required incident flux varies with microwave source configurations, where either one sided or distributed incidence may reduce I_{crit} depending on L_{exp}. Thus, based on Fig. 9, proper microwave source configurations and I_{crit} can be judiciously selected to optimize the experimental parameters. In other words, for fixed oil thickness and total incident flux I_0, proper configurations of microwave sources (ϕ_0) can be selected either to promote or suppress the onset of convection. Similarly, for fixed microwave source configuration and total incident flux (I_{expt} shown in the inset plot), the critical oil thicknesses (L_{crit}) required for onset of convection can be obtained from Fig. 9, as indicated by arrows. It may be noted that for a specified I_{exp}, one can have multiple L_{crit} even for same ϕ_0. Thus, Fig. 9 can be used as guiding curve for determining various experimental parameters in order to control onset of convection during microwave heating of oil.

An important feature related to the onset of convection due to microwave incidence within oil may be observed from

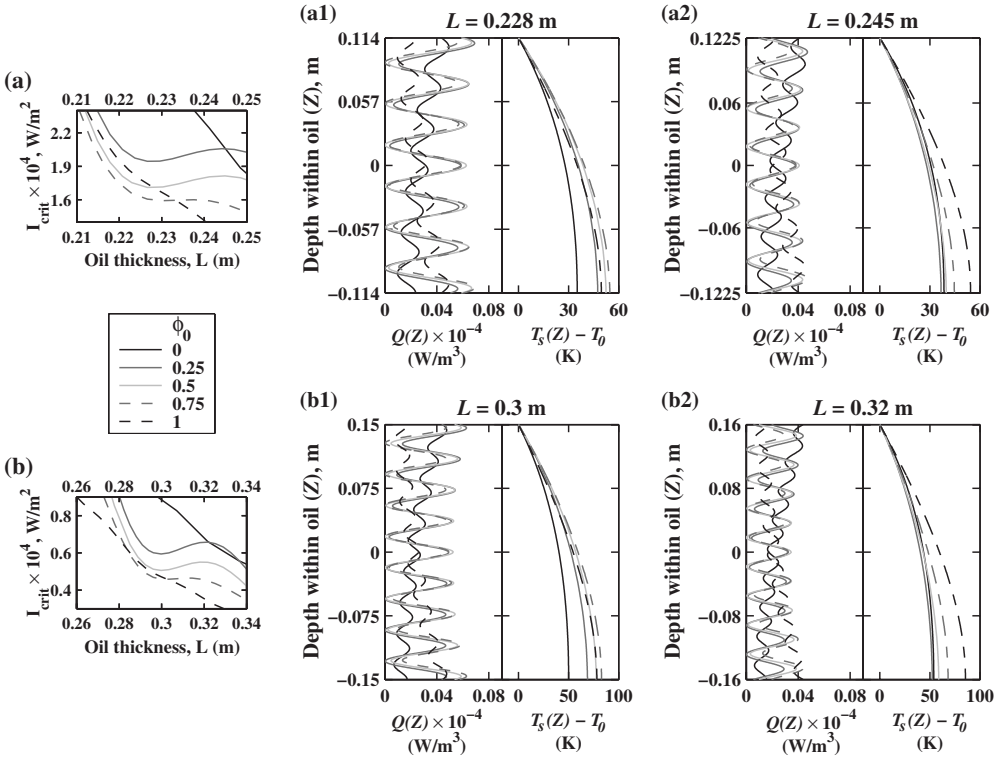

FIG. 10. Local maxima of I_{crit} for selected range of oil thicknesses [$0.21\leqslant L\leqslant0.25$ in subplot (a) and $0.26\leqslant L\leqslant0.34$ in subplot (b)]. The corresponding absorbed power distributions [$Q(Z)$] and base state temperature profiles [$T_s(Z)-T_0$] around the maxima [L=0.245 in subplot (a2) and 0.32 m in subplot (b2)] and minima [L=0.228 in subplot (a1) and 0.3 m in subplot (b1)] of I_{crit} are shown for various microwave source configurations (ϕ_0=0, 0.25, 0.5, 0.75, and 1) with I_0=100 W m^{-2}.

Fig. 9, which shows that I_{crit} exhibits maxima at certain oil thicknesses (within the range of 0.1 m$\leqslant L\leqslant$1 m) for distributed incidences (ϕ_0=0.25, 0.5, and 0.75), while the peaks of I_{crit} disappear for one sided incidences (ϕ_0=0 and 1). The presence of peaks in I_{crit} is in contrary to the onset of the Rayleigh–Benard convection, where I_{crit} decreases monotonically with increasing sample length. Thus, the underlying cause leading to the occurrence of maxima in I_{crit} is further investigated in Fig. 10 for selected ranges of oil thickness, where I_{crit} exhibits maxima. In Fig. 10, the variations of I_{crit} within selected range of oil thicknesses are shown in first column [0.21 m$\leqslant L\leqslant$0.25 m in subplot (a) and 0.26 m$\leqslant L\leqslant$0.34 m in subplot (b)]. It is found that for ϕ_0=0.25, 0.5, and 0.75, I_{crit} exhibits minima around L=0.228 [Fig. 10(a)] and 0.3 m [Fig. 10(b)] while maxima of I_{crit} appear around L=0.245 [Fig. 10(a)] and 0.32 m [Fig. 10(b)]. The corresponding absorbed power distribution [$Q(Z)$] and base state temperature profiles [$T_s(Z)-T_0$] for L=0.228, 0.245, 0.3, and 0.32 m are shown in subplots (a1), (a2), (b1), and (b2), respectively. The absorbed power and base state temperature profiles in Fig. 10 are determined using I_0=100 W m^{-2} and other parameters, as in Fig. 9. It may be seen from subplots (a1), (a2), (b1), and (b2) that for distributed incidences, the microwave power absorption near the bottom surface is higher for L=0.228 and 0.3 m compared to those at L=0.245 and 0.32 m, respectively. This results in higher base state temperature difference between top and bottom plates at L=0.228 and 0.3 m compared to L=0.245 and 0.32 m, respectively, for ϕ_0=0.25, 0.5, and 0.75. Accordingly I_{crit} for distributed incidences is lower for L=0.228 and 0.3 m than those for L=0.245 and 0.32 m, respectively, and I_{crit} exhibits maxima at L=0.245 and 0.32 m for distributed incidences. It may be further noted from subplots (a1), (a2), (b1), and (b2) that the local intensification of absorbed power near the bottom surface at specific oil thicknesses disappear for one sided incidences and I_{crit} does not exhibit any peak for ϕ_0=0 and 1.

As a conclusive remark, this work presents not only the variations of critical Rayleigh and wave numbers with various parameters related to microwave heating of oil but also relate them to the spatial patterns of absorbed power distributions. This work has immense practical important since the onset of convection can be forecasted from the absorbed power profiles and can act as a precursor for the analysis of much complex systems.

ACKNOWLEDGMENTS

The authors would like to thank Anonymous reviewers for critical comments and suggestions which improved the quality of the manuscript.

[1]R. S. Farag, G. El-Baroty, N. Abd-El-Aziz, and A. M. Basuny, Int. J. Food Sci. Nutr. **48**, 365 (1997).
[2]F. Caponio, A. Pasqualone, and T. Gomes, Int. J. Food Sci. Technol. **38**, 481 (2003).
[3]L. X. Xia, S. W. Lu, and G. Y. Cao, Sep. Sci. Technol. **38**, 4079 (2003).
[4]L. Z. Kong, P. Li, Q. K. Zhang, S. L. Zhao, P. Li, and L. H. Zhuang, Pet. Sci. Technol. **24**, 769 (2006).
[5]F. Anjum, F. Anwar, A. Jamil, and M. Iqbal, J. Am. Oil Chem. Soc. **83**, 777 (2006).
[6]W. Tan, X. G. Yang, and X. F. Tan, Sep. Sci. Technol. **42**, 1367 (2007).
[7]H. Shang, S. W. Kingman, C. E. Snape, and J. P. Robinson, Ind. Eng. Chem. Res. **46**, 4811 (2007).
[8]B. Sultana, F. Anwar, and R. Przybylski, Food Chem. **104**, 997 (2007).
[9]S. Zhao, P. Li, and L. Kong, Pet. Sci. Technol. **25**, 1583 (2007).
[10]J. P. Robinson, C. E. Snape, S. W. Kingman, and H. Shang, J. Anal. Appl. Pyrolysis **81**, 27 (2008).
[11]S. A. Barringer, E. A. Davis, J. Gordon, K. G. Ayappa, and H. T. Davis, AIChE J. **40**, 1433 (1994).
[12]T. Basak, AIChE J. **50**, 2659 (2004).
[13]T. Basak and S. S. Kumaran, Chem. Eng. Sci. **60**, 5480 (2005).
[14]T. Basak and A. S. Priya, J. Appl. Phys. **97**, 083537 (2005).
[15]C. A. Vriezinga, J. Appl. Phys. **85**, 3774 (1999).
[16]C. A. Vriezinga, J. Appl. Phys. **79**, 1779 (1996).
[17]K. G. Ayappa, Rev. Chem. Eng. **13**, 1 (1997).
[18]M. Bhattacharya and T. Basak, AIChE J. **52**, 3707 (2006).
[19]M. Bhattacharya and T. Basak, Chem. Eng. Sci. **61**, 6273 (2006).
[20]M. Bhattacharya and T. Basak, Ind. Eng. Chem. Res. **46**, 750 (2007).
[21]E. Jerby, O. Aktushev, and V. Dikhtyar, J. Appl. Phys. **97**, 034909 (2005).
[22]D. F. Soldea, D. Razansky, and P. D. Einziger, J. Appl. Phys. **94**, 2053 (2003).
[23]Q. O. Zhang, T. H. Jackson, and A. Ungan, Int. J. Heat Mass Transfer **43**, 2141 (2000).
[24]T. Basak and K. G. Ayappa, AIChE J. **47**, 835 (2001).
[25]D. P. Mckenzie, J. M. Roberts, and N. O. Weiss, J. Fluid Mech. **62**, 465 (1974).
[26]D. J. Tritton, Nature (London) **257**, 110 (1975).
[27]D. E. Farrow and J. C. Patterson, Int. J. Heat Mass Transfer **36**, 89 (1993).
[28]N. Rudraiah and G. N. Sekhar, ASME Trans. J. Heat Transfer **113**, 122 (1991).
[29]D. J. Tritton and M. N. Zarraga, J. Fluid Mech. **30**, 21 (1967).
[30]P. H. Roberts, J. Fluid Mech. **30**, 33 (1967).
[31]T. Marimbordes, A. O. El Moctar, and H. Peerhossaini, Int. J. Heat Mass Transfer **45**, 667 (2002).
[32]I. S. Shivakumara, M. S. Nagashree, and K. Hemalatha, Int. Commun. Heat Mass Transfer **34**, 1041 (2007).
[33]M. Tveitereid and E. Palm, J. Fluid Mech. **76**, 481 (1976).
[34]E. M. Sparrow, R. J. Goldstein, and V. K. Jonsson, J. Fluid Mech. **18**, 513 (1964).
[35]F. A. Kulacki and R. J. Goldstein, Appl. Sci. Res. **31**, 81 (1975).
[36]S. Saravanan and P. Kandaswamy, ZAMP **55**, 451 (2004).
[37]A. Yücell and Y. Bayazitoglu, ASME Trans. J. Heat Transfer **101**, 666 (1979).
[38]Y. Tasaka and Y. Takeda, Int. J. Heat Mass Transfer **48**, 1164 (2005).
[39]J. Gilchrist, G. A. Kriegsmann, and D. T. Papageorgiou, IMA J. Appl. Math. **60**, 73 (1998).
[40]A. Sander, Chem. Eng. Process. **46**, 1324 (2007).
[41]W. Wang and G. H. Chen, AIChE J. **53**, 3077 (2007).
[42]L. A. Campanone and N. E. Zaritzky, J. Food. Eng. **69**, 359 (2005).
[43]X. Wu, J. R. Thomas, and W. A. Davis, J. Appl. Phys. **92**, 3374 (2002).
[44]G. J. Fleischman, J. Food. Eng. **40**, 81 (1999).
[45]A. R. von Hippel, *Dielectric Properties and Waves* (Wiley, New York, 1954).
[46]W. H. Press, B. P. Flannery, S. A. Teukolskya, and W. T. Vetterling, *Numerical Recipes in FORTRAN 77: The Art of Scientific Computing* (Cambridge University Press, Cambridge, 1992).
[47]W. Heinrichs, Math. Comput. **53**, 103 (1989).
[48]W. Heinrichs, J. Sci. Comput. **6**, 1 (1991).
[49]W. Heinrichs, SIAM (Soc. Ind. Appl. Math.) J. Sci. Stat. Comput. **12**, 1162 (1991).